

The microlensing rate and mass function vs. dynamics of the Galactic bar

Hongsheng Zhao & P. Tim de Zeeuw[?]

Sterrewacht Leiden, Niels Bohrweg 2, 2333 CA, Leiden, The Netherlands^Y

Accepted ::: Received ::: in original form :::

ABSTRACT

With the steady increase of the sample size of observed microlenses towards the central regions of the Galaxy, the main source of the uncertainty in the lens mass will shift from the simple Poisson noise to the intrinsic non-uniqueness of our dynamical models of the inner Galaxy, particularly, the Galactic bar. We use a set of simple self-consistent bar models to investigate how the microlensing event rate varies as a function of axis ratio, bar angle and velocity distribution. The non-uniqueness of the velocity distribution of the bar model adds a significant uncertainty (by about a factor of 1.5) to any prediction of the lens mass. Kinematic data and self-consistent models are critical to lift the non-uniqueness. We discuss the implications of these results for the interpretation of microlensing observations of the Galactic bulge. In particular we show that Freeman bar models scaled to the mass of the Galactic bulge/bar imply a typical lens mass of around $0.8M_{\odot}$, a factor of 3-5 times larger than the value from other models.

Key words: dark matter – gravitational lensing – galactic centre

1 INTRODUCTION

Five years of searches for gravitational microlenses, which significantly increase the brightness of a background source star when they come to the same line of sight by chance, have produced roughly 200 possible microlensing events towards the Galactic bulge/bar from several surveys (e.g., Udalski et al. 1994; Aard et al. 1995; Acock et al. 1997; The expectation is that with more and more events coming in at a steady rate, we will obtain a better understanding of the structure of the Galaxy, and of the mass spectrum of lenses (see Paczynski 1996 for a review). Microlensing is perhaps the only direct method to probe the mass function in the Galactic bulge/bar, in particular the fraction of low luminosity objects (brown dwarfs/M-dwarfs) just below or just above the hydrogen burning limit. These objects are so faint intrinsically ($M_V > 10m_{\text{ag}}$) and so far away (distance modulus of about 14.5 mag) that they are missing in even the deepest star count studies of the bulge/bar with the Hubble Space Telescope (Gould, Bahcall & Flynn 1996).

Several attempts have been made to estimate the typical mass of the observed microlenses (Kiraaga & Paczynski

1994; Zhao, Spergel & Rich 1994; Han & Gould 1996; Mao & Paczynski 1996) on the basis that events last longer for more massive lenses, with m/t^2 , where m is the mass of a single point lens and t is the time for a source on the Einstein ring (where the amplification factor is 1.34) to move to exactly behind the lens. The time scale t can be derived by fitting the light curve of the amplified source, but to convert it to the lens mass m requires knowing other system parameters, including the distances and transverse velocities of the lens and the source. These, unfortunately, are often poorly known from observations. Nevertheless the problem can be partially circumvented if one has a well-determined dynamical model of the inner Galaxy. The missing information can then be simulated by drawing random samples of the lens and the source in a Monte-Carlo fashion from the model phase-space distribution of the inner Galaxy.

With the increase of the event sample size, it becomes meaningful to ask the question whether the whole mass spectrum of the lenses can be determined in the above way (Han & Lee 1997). This requires an understanding of the uncertainty of the underlying dynamical model. Models of the inner Galaxy are, unfortunately, still far from being well-determined and they are subject to constant modifications and improvements, driven by new observations (see e.g., reviews by de Zeeuw 1993; Gerhard 1996). How much the Galactic bar differs from a simple oblate rotator is an unsettled issue. Generally speaking the density distribution of

[?] E-mail: hsz@strw.leidenuniv.nl, tim@strw.leidenuniv.nl

^Y Based in part on work done at the Max-Planck-Institut für Astrophysik, Karl-Schwarzschild-Strasse 1, 85740 Garching, Germany

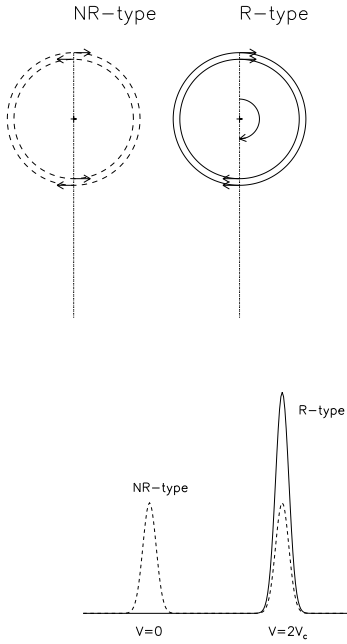


Figure 1. Two simple disc models to the right (R-type model) are rotating models where all stars (lenses and sources) move in the clockwise direction, and models to the left are non-rotating with half of the stars (lenses and sources) orbiting in the clockwise sense, half anti-clockwise. The transverse velocity of the lens and the source at the line of sight to the center (dotted lines) is V_c . The lower panel draws schematic distributions of the relative source-lens speed $V = |v_s - v_l|$ in the simplest case where the lens and the source are at the front or on the back side of an annulus.

the Galactic bar is constrained only up to a one-parameter sequence by the integrated COBE map, with the bar angle being a free parameter (Binney, Gerhard & Spergel 1997; Zhao 1997). Various velocity structures of the bar could also be consistent with the same bar potential (Penny 1984). Schwarzschild-type models for the inner Galaxy (Zhao 1996; Binney et al. 1997) which attempt to fit simultaneously the photometric and kinematic data measurements are still rare.

The observed velocity field of a bar is the result of its tumbling motion, the internal streaming motion on top of the pattern rotation, and the velocity anisotropy. Bars of different pattern speed and/or orbital compositions are indistinguishable in their projected density and optical depth maps, but they differ at the level of event rate and event duration distribution. This is easily seen from the basic equation of microlensing,

$$\frac{1}{t} = \frac{V}{R_E} = V \frac{4GmD}{c^2}^{1/2}; \quad D = \frac{D_1}{D_s} (D_s + D_1); \quad (1)$$

where G is the gravitational constant, c is the velocity of light, R_E is the Einstein ring radius, t is the event duration (one Einstein radius crossing time), D_1 and D_s are the distances to the lens and the source, V is the relative transverse speed between the two, and m is the mass of the lens. For most microlensing events one observes only their duration,

from which one can obtain a lensing probability (optical depth) and an event rate observationally. Other system parameters, such as the speed V and distances D_s and D_1 , can at best be inferred statistically from a phase-space density model of the Galaxy. As a result the rate is related to the dynamical model as follows (cf. eq. [7] of Paczynski 1986)

$$\frac{1}{t} = \frac{2}{t} \frac{D_1 E}{c} = \frac{c}{GmD} \langle v_i \rangle; \quad (2)$$

where the brackets indicate averages. In order to emphasize the effect of the velocity distribution we have fixed the mass of the lenses m and the positions of the lens and source.

Eq. (2) can also be interpreted as a constraint on lens mass. If the event rate is fixed at the observed value and the lens volume density model is fixed to fit the observed optical depth, then eq. (2) implies that

$$m \propto \langle v_i \rangle^2; \quad (3)$$

so that the inferred lens mass is sensitive to the velocity distribution of the dynamical model. An uncertainty of 1:2 in velocity translates to a factor of 1:4 in the lens mass, in which case one could mistake, e.g., an M-dwarf for a brown-dwarf dominated model.

To illustrate this point, it is best to take one step backwards to consider the simplest axisymmetric models. If one observes the two discs shown in Figure 1 edge-on, then the distribution of transverse relative source-lens speed peaks at $V = 2V_c$ for the maximum rotating disc (R-type; R stands for rotator), but peaks at both $V = 2V_c$ and $V = 0$ for the two-stream counter rotating disc (NR-type, standing for non-rotator). Since the median speed $\langle v_i \rangle$ is twice as large in the R-type model as in the NR-type model, twice as many events with duration twice as short are expected in the R-type model as in the NR-type model. In a more realistic situation where lenses and sources are distributed across a uniform disc and they orbit the center at constant angular speed, the R-type model would predict (after a simple calculation) an average speed $\langle v_i \rangle$ and an event rate a factor of 1.2 times longer than in NR-type models.

Past attempts to statistically determine the mass function of microlenses all suffer from uncertainties in the dynamical models of the inner Galaxy. Binney, Gerhard & Spergel (1997) and Zhao (1997) studied volume density models of the Galactic bar consistent with the projected light distribution from the COBE/DIRBE maps, Zhao & Mao (1996, hereafter ZM) addressed the effects of the uncertain volume density model on the microlensing probability (the optical depth). This paper extends such studies to the microlensing event rate distribution. We concentrate on breaking the degeneracy of dynamical models with the same three-dimensional density distribution but different velocity fields, which are indistinguishable in studies based on the projected light and the optical depth.

The main goal of this paper is to study the trend of the microlensing event rate as a function of the key parameters of the bar (the pattern speed, the axis ratio and the orientation angle) assuming a fixed lens mass m . This helps us to gauge whether the lens mass should increase or decrease in case a modification of the bar parameters is required to be consistent with some future observations or dynamical

models. A side result is to give an error bar for predictions of the lens mass due to the non-uniqueness of the bar.

The rigorous way to survey microlensing properties of Galactic bar models is to build many sequences of three-dimensional bar models such as in Zhao (1996) which cover the multi-parameter space. But such heavy numerical modelling would be very inefficient. For a first study it is more interesting to gauge the underlying physical effects with simple theoretical models. In this paper we show which insights can be gained from studying the microlensing properties of the analytical two-dimensional Freeman (1966) bars, which surprisingly capture most of the microlensing effects of a realistic bar fairly well.

The outline of the paper is as follows. In §2, we summarize the properties of the Freeman bars, and we derive the optical depth for self-lensing. In §3, we derive basic scaling relations for the event rate distribution. In §4 we show the run of event rate as functions of bar parameters. In §5 we show how to distinguish Freeman bars with the same projected density and optical depth map, and in §6 we derive the rate for extremely short events. Finally, we discuss implications for the Galactic bar in §7. Some mathematical details are given in the Appendix.

2 SELF-LENSING OF THE FREEMAN BARS

Freeman (1966, hereafter F66) discovered self-consistent tumbling bar models with a known analytical distribution function. These two-dimensional bars have been widely used to gain insight into the structure of general self-consistent bars (Hunter 1974; Tremaine 1976; Weinberg & Tremaine 1983). Despite the two-dimensional nature and the special distribution functions, this class of easy-to-build bars contains the main factors by which bars can affect the microlensing rate. These include its elongated density contours and similarly elongated velocity ellipsoid, plus the pattern rotation and streaming motion. Our aim is to vary these factors and "observe" the bar both at a variable line-of-sight angle from its long axis and at a variable projected radius.

2.1 Freeman bars

The Freeman bar is a two-dimensional inhomogeneous elliptical bar of finite extent, with surface density given by

$$\Sigma(X; Y) = \frac{3M}{2ab} \left(1 - \frac{X^2}{a^2} - \frac{Y^2}{b^2}\right)^{\frac{1}{2}}; \quad (4)$$

and a potential

$$\Phi(X; Y) = \frac{GM}{2(ab)^{\frac{3}{2}}} [A_2(q)X^2 + B_2(q)Y^2]; \quad q = \frac{b}{a}; \quad (5)$$

where M is the total mass, a and b are the semi-major (X) and semi-minor (Y) axes of the bar, and $A_2(q)$, $B_2(q)$ are dimensionless function of the axis ratio q given in equation (2) of F66. The symmetry axes (X and Y) rotate with an angular speed Ω with respect to the rest frame. For a given density, there is a sequence of self-consistent models with different amounts of pattern rotation. The sequence is a function of $\Omega = \Omega_J$, where

$$\Omega_J^2(M; a; b) = \frac{GM}{(ab)^{\frac{3}{2}}} \frac{q^1 A_2}{q^1} \frac{q B_2}{q}; \quad (6)$$

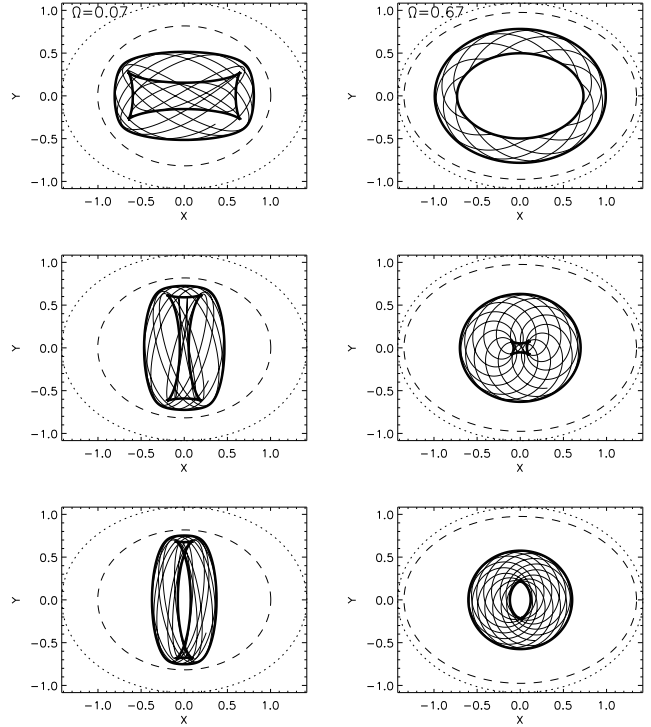


Figure 2. Orbits in Freeman bars with $GM = 1$ and semi-axes $a = 1.420$ and $b = 1.084$ and a boundary as indicated with the dotted ellipses in each panel. The orbits are drawn in the $X - Y$ frame corotating with the tumbling bar with a pattern rotation speed $\Omega = 0.07$ (left panels) and 0.67 (right panels). All orbits are assigned the same Jacobi integral $E_J = 0.5$, which confines the orbits within the zero velocity curves shown as the dashed ellipses in each panel. The heavy solid lines indicate the boundaries of each orbit, as given in Appendix A.

is so defined that when $\Omega = \Omega_J$ the bar is of Jacobi type, that is, with neither internal streaming motion nor velocity anisotropy.

The potential (5) is that of a two-dimensional anisotropic harmonic oscillator with generally incommensurable frequencies in the X and Y directions. The motion is separable in canonical coordinates $(P_1; P_2; Q_1; Q_2)$ defined by F66. Accordingly, all orbits have two independent isolating integrals of motion, and they are in fact rectangular Lissajous figures in the $(Q_1; Q_2)$ -plane. In the corotating $(X; Y)$ -frame, the orbits show a more interesting variety of shapes, similar to what is seen in more general bar potentials. We illustrate these in Figure 2. The boundary curves of each orbit can be worked out analytically. We give the equation in Appendix A. For the fast tumbling bar, the orbits range from direct to retrograde. As the tumbling frequency approaches zero, all orbits become rectangular boxes. By properly weighting orbits with different size and axis ratio, F66 was able to produce a self-consistent elliptical bar. Its distribution function, which is positive definite, has the simple form

$$f(J) = \begin{cases} f_0 (1 - J)^{\frac{1}{2}}; & \text{if } 0 \leq J \leq 1, \\ 0 & \text{otherwise.} \end{cases} \quad (7)$$

Figure 3. The different coordinate systems used. $x = 0$ along the heavy dashed line.

The analytical expression for J is fairly lengthy, but is essentially a linear combination of the two energy integrals, and is given in equations (43)-(45) of F66.

The system has a very simple velocity distribution. In the frame rotating with the bar, stars stream in the retrograde sense with elliptical stream lines concentric to the bar's boundary. The velocity ellipsoid is generally anisotropic with them a x axis either in the X or Y direction. The amplitude of the streaming motion is linear with respect to the coordinates, and the amplitude of the dispersions decreases to zero with a radial dependence $\propto (1 - |x|)^2$, identical to that of the surface density given in eq. (4). A self-consistent Freeman bar model is fully specified by its mass M , the semi-axes a , b and the pattern speed Ω . One can construct a sequence of bar models from needle-shaped to axisymmetric by varying the axis ratio b/a . By varying only $\Omega = \Omega_j$ one can build a sequence of models with the same density distribution but different velocity anisotropy and streaming motions.

2.2 Distributions of the transverse velocity and the density in the line of sight

The microlensing rate of the bar is determined by the distributions of the transverse velocity and the three-dimensional volume density in the line of sight path to a source. We assume that the observer is sufficiently far away from the center of the Freeman bar that all perspective effects can be ignored. Even though this makes the analytical studies here not rigorously applicable to the Galaxy, where perspective effects are a main clue to the size and orientation of the bar, it still provides very useful insights.

The density distribution depends on the thickness of the bar, on the orientation of the bar and on the impact parameter of the line of sight of the observer. To modify the 2D Freeman bar to a three-dimensional model, we assume

the Freeman bar by a small constant thickness z , so that the volume density distribution is given by^Z

$$\rho(x, y, z) = \frac{\rho(x, y)}{z}; \quad \text{min}(a, b): \quad (8)$$

We use a Galactocentric Cartesian coordinate system (x, y, z) with the x -axis pointing away from the Sun, making an angle ψ with the bar's long (X) axis. Similar but more convenient is the following coordinate system $(\tilde{x}, \tilde{y}, z)$ with

$$\tilde{x} = x - C y; \quad C = \frac{(q - q^{-1}) \sin \psi \cos \psi}{q \cos^2 \psi + q^{-1} \sin^2 \psi}; \quad (9)$$

so that it is obtained by applying a shear to the original (x, y, z) coordinate in the line-of-sight direction, as illustrated in Figure 3. In these coordinates the face-on density of the Freeman bar can be rewritten as

$$\rho(\tilde{x}, y) = \frac{3M}{2ab} \left(1 - \frac{\tilde{x}^2}{d_0^2} - \frac{y^2}{y_0^2} \right)^{\frac{1}{2}}; \quad (10)$$

where $2y_0$ and $2d_0$ are the projected width and the central depth of the bar. Both quantities are functions of a , b and ψ , given by

$$y_0 = (ab)^{\frac{1}{2}}; \quad d_0 = \frac{ab}{\sin \psi}; \quad (11)$$

with

$$\sin \psi = \frac{q}{q^2 + 1}; \quad (12)$$

A line of sight with an impact parameter y intersects with the bar's near end at $\tilde{x} = -d(y)$ and far end at $\tilde{x} = +d(y)$, where

$$d(y) = d_0 \left(1 - \frac{y^2}{y_0^2} \right)^{\frac{1}{2}}; \quad (13)$$

so that $2d(y)$ is the depth of the bar at y . For an axisymmetric disc, $a = b = y_0 = d_0 = \frac{ab}{\sin \psi} = \frac{ab}{q}$, and $\psi = 90^\circ$.

The transverse velocity distribution depends on the velocity field of the bar, the orientation and the impact parameter of the line of sight. It is given by a box car distribution:

$$P(v_y) = \int_{-d(y)}^{+d(y)} f(J) dv_x \quad (14)$$

$$= \begin{cases} \frac{1}{2w} & \text{if } |v_y - v_j| \leq w, \\ 0 & \text{otherwise,} \end{cases}$$

where the local transverse streaming velocity v is a linear function of (\tilde{x}, y) , and the half width w is $\frac{1}{3}$ times the local transverse dispersion, which is proportional to $(1 - |x|)^{\frac{1}{2}}$. v can be split into a component v_x proportional to \tilde{x} and a (less useful) component proportional to y . More rigorously

$$\frac{v_x}{v} = \frac{\tilde{x}}{d(y)}; \quad \frac{v_y}{v} = \frac{p}{3} \left(1 - \frac{\tilde{x}^2}{d^2(y)} \right)^{\frac{1}{2}}; \quad (15)$$

^Z The non-axisymmetric perturbation in the COBE/DIRBE map of the Galaxy has a thickness no less than the thin disc ($z > 200$ pc) and semi-minor axis no greater than the corotation radius ($b < a < 4$ kpc) so the requirement that $z/b \ll 1$ is barely satisfied.

where we have rescaled the x coordinate by $d(y)$, the y coordinate by y_0 and the velocities by $v(y)$, which is defined as

$$v(y) = v_0 \left[1 - \frac{y^2}{y_0^2} \right]^{\frac{1}{2}}; \quad (16)$$

and $v_0 = v(y=0)$ is the central transverse dispersion. The parameter β is defined by

$$\frac{\beta}{a}; \quad \frac{v_{\text{max}}}{v_0}; \quad (17)$$

where v_{max} is the transverse rotation speed at $x = a$ along the $y = 0$ line. So β is a dimensionless global (independent of y) indicator of the amount of rotational support in the system (similar to the conventional V_{rot} parameter, e.g., Binney & Tremaine 1987). Both v_0 and β are lengthy functions of the bar axis ratio and pattern speed, which are given in Freeman (1966) in the case that the bar angle $\theta = 0^\circ$ or 90° . The dependence on β is then easily worked out with

$$\frac{v_0(\theta)}{v_0(0)} = \frac{v_0(0)}{v_0(90)} \frac{\cos^2 \theta}{\sin^2 \theta}; \quad (18)$$

For our purpose it is only important to know that for a non-rotating bar $\beta = 0$ and the velocity ellipsoid is aligned with the bar; for a Jacobi-type rotator ($\theta = 45^\circ$), stars have an isotropic dispersion on top of a solid body pattern rotation with respect to the rest frame.

More relevant to the microlensing is the lens-source relative transverse speed V and its distribution $F(V)$, which is a convolution of the distribution $P(v_y)$ of eq. (14) for the transverse velocity distribution of the lens or the source.

$$F(V) = \int P(v_y) [P(v_y - V) + P(v_y + V)] dv_y; \quad (19)$$

where we have integrated over the source velocity v_y . The integration can be carried out, but the result is somewhat lengthy, and is given in eq. (B1). We remark that $F(V)$ satisfies the normalization $\int_0^\infty F(V) dV = 1$.

2.3 Optical depth

Following ZM, we assume that the sources are distributed with a number density proportional to the mass density ρ_s , which is in turn proportional to ρ_1 . Then the lensing optical depth averaged over all sources along the line of sight with impact parameter y is

$$\tau(y) = \int_{d(y)}^{+Z} \rho_s \frac{dZ}{d_s} \int_{d(y)}^{+Z} \rho_1 \frac{dZ}{d_s} dx_s; \quad (20)$$

where

$$d_s = \frac{4G}{c^2} (\rho_s \rho_1) d_1; \quad (21)$$

is the optical depth for a source located at $(x_s, y; 0)$, and d_1 is the volume density at the lens position. Here the subscripts s and 1 denote quantities of the source and the lens, respectively. For the Freeman bar:

$$\tau(y) = \frac{128G}{15c^2} \frac{M}{d_0} \frac{1}{d_0} \left[1 - \frac{y^2}{y_0^2} \right]^{\frac{3}{2}}; \quad (22)$$

3 EVENT RATE DISTRIBUTION

3.1 Definitions

The duration of a microlensing event is related to the lens mass m and to the relative distance $x_s - x_l$ and velocity V between the lens and the source by (cf. eq. 1)

$$t = \frac{r}{V} \frac{4Gm}{c^2} (x_s - x_l); \quad (23)$$

where we have made the approximation $D \approx x_s - x_l$ for self-lensing of a far-away bar. If one fixes the lens mass m and the source position x_s , then the probability of observing an event with any duration is the optical depth d_s (cf. eq. 21). But only the fraction $F(V)dV$ of the lenses with relative velocity V to $V + dV$ contributes to the event with duration t to $t + dt$, where $F(V)$ is the relative velocity distribution given in eq. (19). So the contribution d to the event rate is

$$d = \frac{2}{t} d_s F(V) dV; \quad (24)$$

where $2 = \langle t \rangle$ is the average frequency of an event with time scale t , and $2 = \frac{A}{\pi}$ is the ratio of the Einstein diameter to the area in dimensionless units (Paczynski 1991). It follows that the differential duration distribution is given by

$$\frac{d}{d \log t} = \frac{2 \ln 10}{t} d_s F(V) V; \quad (25)$$

Just as for the case of the optical depth (20), the observable rate should be averaged over the source distribution along the line of sight. We define the microlensing duration distribution profile $f(\log t)$ normalized by the optical depth as

$$f(\log t) = \frac{d}{d \log t}; \quad (26)$$

so that

$$\int f(\log t) d \log t = 1; \quad (27)$$

where \int is the total event rate. Then the source density averaged duration profile is given by (cf. eqs 20 and 21)

$$f(\log t) = \frac{\int_{d(y)}^{+Z} \rho_s \frac{dZ}{d_s} \int_{d(y)}^{+Z} \rho_1 \frac{dZ}{d_s} dx_s \int_{d(y)}^{+Z} \rho_s \frac{dZ}{d_s} dx_s \int_{d(y)}^{+Z} \rho_1 \frac{dZ}{d_s} dx_s}{\int_{d(y)}^{+Z} \rho_s \frac{dZ}{d_s} \int_{d(y)}^{+Z} \rho_1 \frac{dZ}{d_s} dx_s} : \quad (28)$$

Note that $f(\log t)$ is independent of the bar thickness Z .

3.2 Scaling relations

The normalized event duration distribution $f(\log t)$ should have the dimension of a to-be-defined typical frequency ν , multiplied by a function of the dimensionless time t . We write this concisely as

$$f(\log t) = \nu(t); \quad (29)$$

where

$$\frac{\nu(t)}{[\frac{Gm}{c^2} d(y)]^{\frac{1}{2}}} = \frac{\nu_0}{[\frac{Gm}{c^2} d_0]^{\frac{1}{2}}} \left[1 - \frac{y^2}{y_0^2} \right]^{\frac{1}{4}}; \quad (30)$$

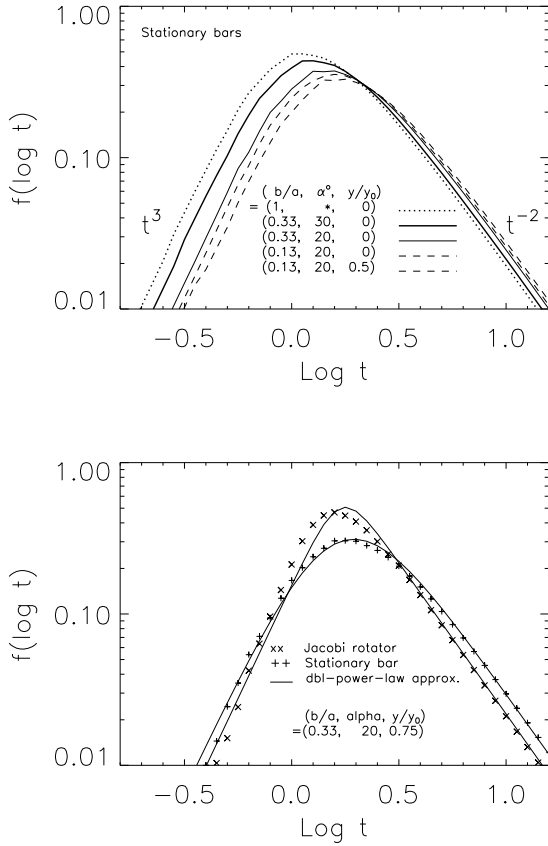


Figure 4. Upper panel: the event duration distribution for stationary Freeman bars with various axis ratio, angle, and impact parameter (b/a ; α ; y/y_0); the curves are labeled in the sequence of their peak positions (from top left to bottom right). The curves all have the same shape, in particular, the same asymptotic power-laws for very short $f(\log t) / t^3$ or very long events $f(\log t) / t^{-2}$. Lower panel: a Jacobi-type rotating model ($\alpha = \alpha_j$) compared with a non-rotating one ($\alpha = 0$), and the simple double-power-law approximation to the distribution (cf. eq. 35). The rotating models have a narrower distribution and higher rate.

and $1 = \tau$ is a typical time scale for the events, α is the ratio of rotation vs. random motion in the model, and $g(\alpha)$ is a dimensionless function of whose functional form depends only on α , which is a dimensionless function of b/a , $\alpha = \alpha_j$, and y/y_0 . The exact derivation of how $f(\log t)$ depends on α is given in Appendix B.

Eq. (29) can be understood intuitively as follows. Consider a line of sight with impact parameter y to a stationary Freeman bar model. The lens-source distance ($x_s - x_l$) scales with the bar's depth $d(y)$, and the transverse velocity V scales with the dispersion $\sigma(y)$ (cf. eq. 15). So the Einstein radius $R_E \propto [m d(y)]^{1/2}$ and the event rate scale with $\frac{1}{\tau} = \frac{V}{R_E} \propto \frac{\sigma(y)}{[m d(y)]^{1/2}}$. As a result, the event duration distribution depends on the bar density parameters, angle and impact parameter only through α . For rotating bars, the profiles also depend on the dimensionless quantity α .

A surprising but direct result of the scaling relation eq. (29) is that all non-rotating Freeman bars have the same "shape", as illustrated in Fig. 4. This means that although

the $\log t$ vs. $\log f$ diagram of models with the same α have different median event duration and total rate, they will coincide after shifting the zero points in both axes by a constant $\log \tau$. In particular, there is a one-to-one correspondence between a non-rotating Freeman bar with a non-rotating Kalnajs (1976) disc, which is an axisymmetric version of the Freeman bar.

Interestingly the event duration distributions of all Freeman bars with the same α also should have the same "shape". The shape is a function of α only. For non-rotating models $\alpha = 0$. One can always find a Kalnajs disc with the same rotation-to-dispersion ratio (α) and the same shape of the microlensing event duration distribution. Just as for the dimensionless $\frac{b}{a}$; $\frac{\alpha}{\alpha_j}$, the width of the event duration distribution depends on the bar angle and axis ratio directly, but depends on the size and mass of the bar only through the normalized pattern speed $\alpha = \alpha_j (M/a; b)$.

The shape of the event duration profiles is also invariant when the same bar model is viewed at different impact parameters because the global parameter α is independent of the impact parameter y (cf. Fig. 4).

3.3 Asymptotic behaviour

Now we consider the asymptotic behavior of the event time scale distribution. The asymptotic power-law profiles are evident in Figure 4. This is because very short events come from a pair of lens and source which are very close in distance, and very long events happen if they are very close in proper motion. Mao & Paczynski (1996) show that this results in two generic power-law profiles for $f(\log t)$ at very small or large values of t for three-dimensional models. Similar to these authors, we found the following asymptotic relations for the two-dimensional Freeman bar,^x

$$\frac{1}{t} f(\log t) = g(t) \quad (31)$$

$$\propto \frac{108 \ln 10}{35} (t)^3 \quad t \ll 0; \quad (32)$$

$$\propto \frac{108 \ln 10}{35} (t)^5 (t)^2 \quad t \gg 1; \quad (33)$$

where g is a dimensionless function of α with $g(0) = 0.94$ (cf. eq. [36]).

The full profile of $f(\log t)$ can be constructed, approximately, by interpolating between the asymptotic relations

$$\frac{1}{t} f(\log t) = g(t) \quad (34)$$

$$\frac{108 \ln 10}{35} (t)^3 \left(1 + \frac{1}{p} \right)^{5p}; \quad t; \quad (35)$$

where p is a measure of the width of the distribution. Both p and g are weakly decreasing functions of α . We find that

$$p(\alpha) \approx 0.36 \left(1 + \frac{2}{\alpha} \right); \quad g(\alpha) \approx 0.94 \left(1 + \frac{2}{\alpha} \right)^{\frac{1}{3}}; \quad (36)$$

^x for very long duration, $f(\log t)$ generally is proportional to $(t)^{\dim}$, where \dim is the dimension of the system. So for three-dimensional bars, $\frac{1}{t} f(\log t) / (t)^3$ when $t \gg 1$.

together with eq. (35), give a reasonably good approximation to $f(\log t)$, good within 10% for non-rotating Freeman bars ($\alpha = 0$) (cf. Fig. 4). Using this interpolation, we find that $\log t$ has a mean at approximately $0.14 \log$ dex with an rms width approximately $0.32 \log$ dex; both the mean and the width are also weak functions of α .

The function $f(\log t)$ is independent of α or rotation for very short events because the lens and source of these events are very close in distance, so their relative rotation speed is always zero. The short duration events are particularly useful for constraining the mass of the lenses in the bar because lenses in the foreground disc are generally sufficiently far away from the sources in the bar that they do not contribute significantly to the short events.

Compared to non-rotating models, the $f(\log t)$ profiles are slightly narrower for models with increasing rotation. This can be understood as a smaller spread in the velocities of lens and source in rotating models leads to a smaller spread of the event duration. However, the variation of the width is small (see Fig. 4), and to good approximation Freeman bars all have very similar $f(\log t)$ profiles.

4 THE TOTAL EVENT RATE AS FUNCTION OF THE BAR PARAMETERS

4.1 The size and mass of the bar

The total event rate per optical depth is given by eqs. (27) and (29):

$$\dot{N} = \int_0^Z g(t) d(\log t) = \dot{N}_0 f(\alpha); \quad (37)$$

where $f(\alpha)$ is a dimensionless increasing function of α . We find

$$f(\alpha) \approx 0.4 \left(1 + \frac{\alpha^2}{5} \right); \quad (38)$$

Eq. (37) shows that \dot{N} is a function of α and only, and it is proportional to \dot{N}_0 . We now show that several useful relations follow from eqs. (37) and (29).

The event rate scales with the lens mass M , the bar mass M_{bar} , size L_{ab} , and thickness L . We define the following characteristic lens-source velocity V , Einstein radius R_E , and frequency ν ,

$$V = \frac{r}{L} \sqrt{\frac{GM}{L}}; \quad (39)$$

$$R_E = \frac{r}{c} \sqrt{\frac{Gm}{c^2}} L; \quad \frac{V}{R_E} = \frac{c}{L} \sqrt{\frac{M}{m}};$$

Then

$$\dot{N} / \dot{N}_0 = \frac{c}{ab} \sqrt{\frac{M}{m}}; \quad (40)$$

Upon substitution in eq. (20), we find the following scaling relation for the optical depth and the event rate,

$$\tau / \tau_0 = \frac{GM}{c^2} \sqrt{\frac{r}{L}}; \quad \dot{N} / \dot{N}_0 = \frac{GM}{c} \sqrt{\frac{M}{ab}} \sqrt{\frac{M}{m}}; \quad (41)$$

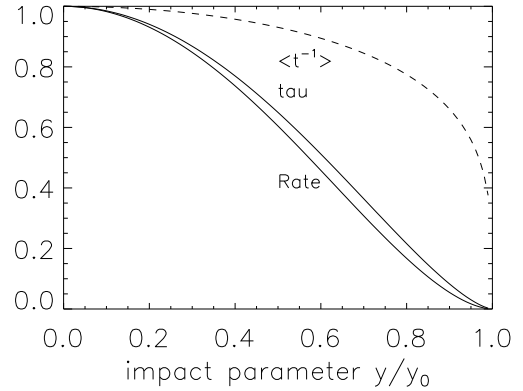


Figure 5. The optical depth, event rate, and event rate per optical depth (scaled with values at $y = 0$) as functions of the impact parameter y . The behavior is the same for all Freeman bars.

For a compact bar with high M or low ab , the velocity dispersion is high, so the event duration is shortened, and the event rate is increased as expected.

4.2 The impact parameter of the line of sight of the observer

Moving away from the center within a model, the event rate drops faster than the optical depth, mostly as a result of a lower escape velocity at large radii, so that the mean event duration $\langle t \rangle^{-1}$ shifts towards larger values (cf. eq. 29, and Fig. 5). Specially:

$$\dot{N} / \dot{N}_0 \propto \frac{y^2}{y_0^2}^{\frac{3}{2}}; \quad (42)$$

$$\tau / \tau_0 \propto \frac{y^2}{y_0^2}^{\frac{7}{4}}; \quad (43)$$

$$\langle t \rangle^{-1} / \langle t \rangle_0^{-1} \propto \frac{y^2}{y_0^2}^{\frac{1}{4}}; \quad (44)$$

However, the shape of the duration distribution profile is always independent of the impact parameter (cf. eq. 29 and Fig. 4).

4.3 The bar axis ratio and orientation angle

For the same bar axis ratio, and the same amount of rotational support (say $\alpha = 0$ as for stationary bars), the optical depth and the event rate increase if the bar points closer to the line of sight, but the events are longer (cf. Fig. 6). This is because when the bar points towards us, it is longest in the line of sight, and smallest in transverse velocity (motions are primarily along the long axis). As a result, both the Einstein radius and the event duration are at their maximum. Figure 6 also shows that the event rate is significantly higher for a rotating model than for a stationary bar with the same axis ratio and bar angle.

At a fixed angle less than 45° , there is an optimal axis ratio (near $b/a = \tan \alpha$) for the bar to yield the highest rate

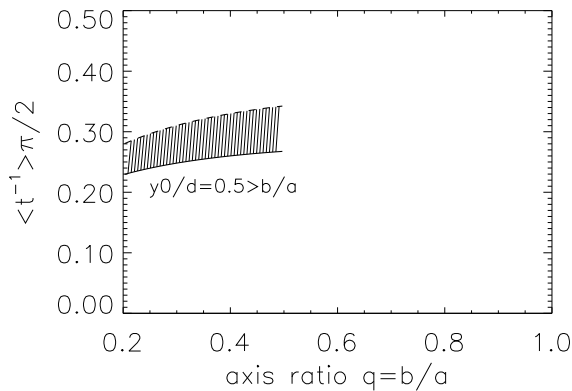
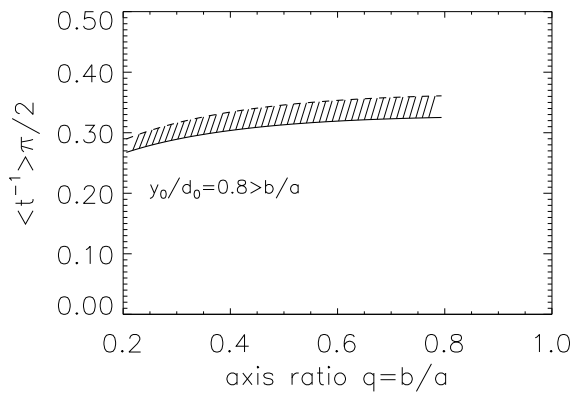
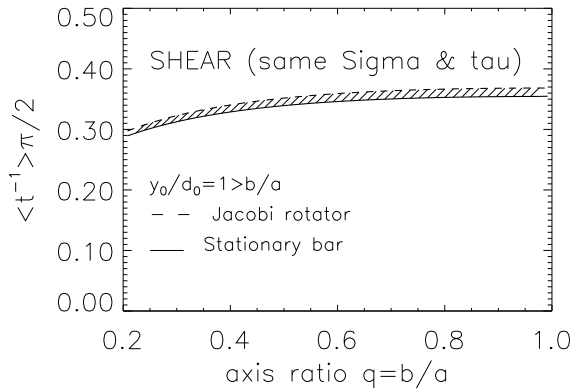


Figure 7. The event rate as a function of the axis ratio for a sequence of three bars related by a shear along the line of sight with a fixed depth to width ratio $d_0=y_0 = 1$. The shaded areas show the spread by bars with different pattern speed. The rates are all for a line of sight through the center of the bar. The optical depth and the surface density is invariant in the sequence (cf. eq. 20).

axisymmetric model satisfies $d_0=y_0 = 1$. A sequence with

{ For these models $b=a = \tan^2$ and the optical depth is the same as for the axisymmetric model, while bars with maximum optical depth have $b=a = \tan$, and the optical depth is enhanced by $1 = \sin^2$ (ZM).

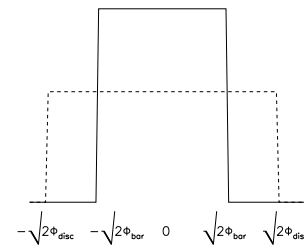
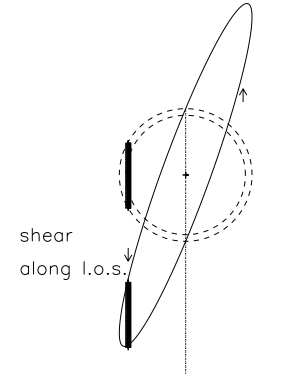


Figure 8. A bar model made by shearing an axisymmetric model along the line of sight direction. For any line of sight, the shear moves the centroid of the mass distribution without changing the amount of lens and source, and their relative distance in the line of sight, so the projected density and the optical depth do not change from model to model. The lower panel draws schematic distributions of the transverse speed at the center (the plus symbol) for a non-rotating bar or disc. The elongated bar has a shallower potential and lower escape velocity $\sqrt{2\phi_{bar}(0)}$ than the disc $\sqrt{2\phi_{disc}(0)}$, where ϕ is the gravitational potential.

$d_0=y_0 > 1$ produces more optical depth than an axisymmetric model, while a sequence with $d_0=y_0 = 1 < 1$ produces less. This is because $\phi / 1 = \phi = d_0=y_0$ (cf. eqs 12 and 20). The observed high optical depth towards the bulge suggests that $d_0=y_0 > 1$ for the Galactic bar, that is, it is longer in depth than across.

Among bars related by a shear transformation, the rate becomes smaller when the bar's axis ratio decreases ($b=a \rightarrow 0$), as a result of shallower potential and smaller velocities. The rate is largest when the axis ratio is maximum and the bar points towards or perpendicular to the observer (Fig 7). The velocity in a needle-shaped bar is close to zero, and so is the event rate. However, excluding such extremely elongated bars which are likely unstable, we find that for bars with $d_0=y_0 = 1 > 1$ the rate is only a weak function of axis ratio; the fractional change is less than 20%.

6 THE RATE OF EXTREMELY SHORT EVENTS

As mentioned in §3, the lenses in the bar dominate the events at the short duration end. The event distribution is a power-law for small t (cf. eq. 32). To quantify the rate of these

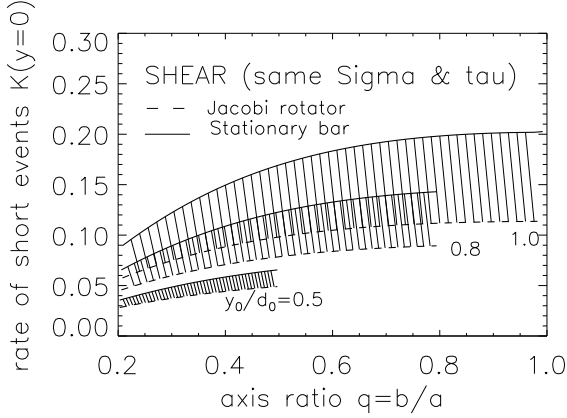


Figure 9. The rate of short events as a function of the axis ratio for a sequence of bars related by a shear in the line of sight with a fixed depth to width ratio $= \frac{y_0}{d_0} = 1;0.8;0.5$ from the top shaded areas to the bottom. The shaded areas show the spread by bars with different pattern speed. The rates are all for a line of sight through the center of the bar. The optical depth and the surface density is invariant in the sequence. (cf. eq. 20).

events, we consider the accumulative event rate for events shorter than t ,

$$\langle t \rangle = \int_0^t f(\log t) d(\log t) \quad (47)$$

where for the Freeman bar the coefficient K is given by

$$K = \frac{36}{35} \frac{M}{m^2} \quad (48)$$

It follows that $\langle t \rangle_{t!0}$ is also a power-law of t with slope 3 (cf. Mao & Paczynski 1996). The expression of K shows two properties: (a) $\langle t \rangle_{t!0}$ is independent of the rotation parameter. (b) $\langle t \rangle_{t!0}$ is very sensitive to $\frac{y_0}{d_0}$.

It is straightforward to repeat the analysis of eq. 47 for the total rate but now for K , since

$$\frac{K}{m^2} \frac{1}{a^4} = \frac{1}{5} \left(1 + \frac{2}{5} \frac{a^2}{b^2} \right) \quad (49)$$

For example,

$$\frac{K}{m^2} \frac{1}{a^4} = \frac{1}{m^2} \frac{M}{ab^2} \left(1 + \frac{y_0^2}{Y_0^2} \right); \quad (50)$$

where $(\frac{y_0}{d_0}; \frac{b}{a})$ is given in equation (12). The general result for extremely short events is that both $\langle t \rangle_{t!0}$ and K are very sensitive functions of the bar parameters $(M; a; b; \frac{y_0}{d_0})$ and the impact parameter y .

The value of K can easily vary by a factor of $(1.2; 1.3)^4 = 2.3$ among models with the same projected density and optical depth (cf. Fig. 9). This implies that the mass moment $\frac{1}{m^2}$ of the lenses in the bar is poorly determined unless kinematic data are used to break the degeneracy of models with the same projected density and optical depth. To clarify this point, it is helpful to rewrite eq. (48) as

$$\frac{1}{m^2} \frac{1}{a^4} = \frac{35}{36} \frac{G^2 d_0^2}{c^2} t^3 \langle t \rangle_{t!0} / \frac{1}{a^4}; \quad (51)$$

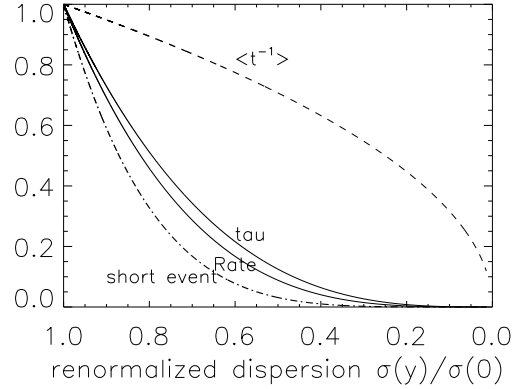


Figure 10. Dependence of lensing properties on the impact parameter of the line-of-sight. The horizontal axis is chosen to be the run of velocity dispersion from the maximum to zero instead of the conventional run of the impact parameter y from the center outwards (but cf. eq. 16 and eq. 5) because in this way the curves are likely to be valid also for more general bars as well. The event time scale (dashed line) increases slowly from the center outwards, but the rate of very short events (heavy dot dashed line) falls off sharply. The optical depth and the total rate are in between these two.

So the extremely sheared and/or rotating models, which have a lower $\frac{y_0}{d_0}$, give a higher estimate of $\frac{1}{m^2}$. This can significantly influence the determination of the lens mass spectrum at the faint end (Mao & Paczynski 1996).

$\langle t \rangle_{t!0}$ follows the general trend of the total rate with the bar mass and size and the impact parameter but with a steeper gradient (cf. Fig. 10). The dependence on the bar angle and the axis ratio is somewhat different from the total rate (cf. Fig. 6 and 11). $\langle t \rangle_{t!0}$ is largest for an oblate model (cf. Fig. 11), which does not exactly follow the general trend of the optical depth.

The main difference with the behaviour of $\langle t \rangle_{t!0}$ is that $\langle t \rangle_{t!0}$ decreases with rotation while the total rate increases. This is because as more kinetic energy is put into rotation, the dispersion σ_0 is lowered, so $K / \frac{1}{a^4} / \frac{1}{a^4}$ (cf. eq. [29]) is lowered.

7 CONCLUSIONS AND IMPLICATIONS FOR THE GALACTIC BAR

We have evaluated the event rate, as well as the event duration distribution and the optical depth, for a family of bar models known as the two-dimensional Freeman bars. We presented several analytical formulae which show the dependence of the optical depth and event rate on the bar mass, size, axis ratio, pattern speed, the bar angle and the impact parameter with a given line of sight. Models with the same optical depth and projected density make slightly different predictions on the event rate and the event duration distribution for a fixed lens mass. Here we consider the implications for the bar in the center of the Galaxy.

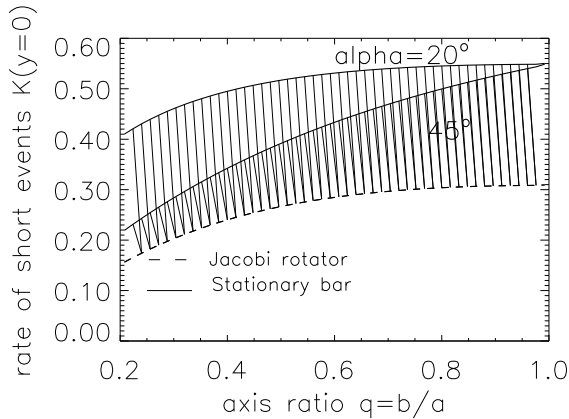


Figure 11. The rate of short events as a function of the axis ratio for a sequence of bars with a fixed bar angle. The shaded areas show the spread by bars with different pattern speed. The Jacobi-type rotators (dashed line) are also isotropic, so $K \propto \frac{4}{0}$ is the same for the two bar angles. The rates are all for a line of sight through the center of the bar.

7.1 Event rate as functions of the bar parameters

Can we reliably generalize the results for the event rate of the Freeman bars to the Galactic bar? Realistic bars are three dimensional and their density structure cannot be modelled by the Freeman disc. Furthermore, the orbits in a realistic bar potential have more variety (e.g., Pfenniger 1984) than in the Freeman bars. For the Galactic bar, it is most interesting to consider models which can fit both the COBE map and the observed optical depth. The Freeman bars certainly are too simple to model these.

Nevertheless the Freeman bars should be able to offer some insights and serve as a reference to more complex systems. The trends found here for the event rate can be extrapolated with some modifications. In particular some of the results are due purely to geometry, e.g., the event rate and duration as functions of the bar angle. Some are generic, e.g., the asymptotic power-laws of $f(\log t)$; the slope at the short duration side is 3 for both two-dimensional and three-dimensional models. Others, e.g., the radial increase of the event duration, and radial falloff of the event rate and optical depth are natural results of a density gradient and the radial falloff of velocity dispersion; the gradient of ρ and σ will depend sensitively on the density gradient. Because the event rate is related to the bar dynamics by several integrations in the lens-source velocity and volume space, which smooth out details of the phase space, only geometrical or generic effects will show up in the event rate. So although true three-dimensional bars have phase-space distribution functions that may be quite different from those of the simple Freeman bars, we expect that the latter will match the basic microlensing physics in the more realistic models.

7.2 Uncertainty of predicting the lens mass

How severe is the non-uniqueness of the lens mass spectrum? The common way to derive the mass spectrum in the COBE bar using microlensing is to compute first an event distribution $f(\log t)$ for a lens with mass m with a given dynamical

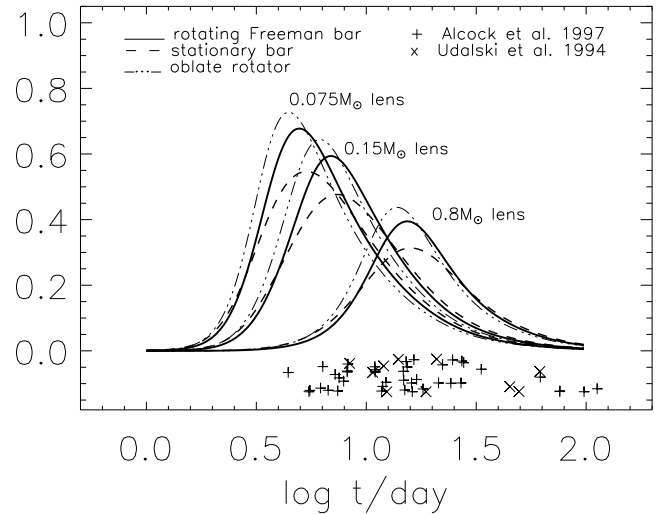


Figure 12. Distribution of the Einstein radius crossing time of the latest hundred or so observed microlensing events towards the bulge, including earlier published data of the MACHO (+ symbols) and OGLE (x symbols) teams. Also shown are predictions for a line of sight towards the center from some simple models with the lens mass being $0.075; 0.15$ or $0.8M_{\odot}$ and the detection efficiency crudely taken into account. The three underlying dynamical models are an oblate rotating Kalnajs (1976) disc with semi-axes $a = b = 1.5 \text{ kpc}$ (....), and a simple Freeman (1966) bar pointing $\theta = 30^{\circ}$ from our line of sight with semi-axes $(a;b) = (1 \tan \theta; \tan \theta) = 1.5 = (2.5; 0.8) \text{ kpc}$ in the rotating case (—) and the non-rotating case (---). All models have the same mass $M = 2 \times 10^6 M_{\odot}$, projected size $10^{\circ} \times 1.5 \text{ kpc}$ and line-of-sight depth 1.5 kpc , so to yield almost indistinguishable maps of the surface density and optical depth.

model of the bar, and then to convolve it with such a mass spectrum that the result fits the observed distribution (e.g., Mao & Paczynski 1996). Any non-uniqueness of the dynamical model propagates to $f(\log t)$, which in turn propagates to the mass spectrum.

The current best estimates of the lens masses, which use realistic models for the Galactic bulge or bar, indicate masses near $0.15M_{\odot}$, with an uncertain but small $< 30\%$ fraction below the hydrogen burning limit (Zhao, Spergel & Rich 1995; Zhao, Rich & Spergel 1996; Han & Gould 1996; Han & Lee 1997). If these results were insensitive to the adopted density profile and flattening of the bar, then a comparable result would be expected from the Freeman bars. But if one simply scales up the Freeman bar models to the often quoted mass and size of the Galactic bulge/bar, and makes a straightforward prediction of the event distribution (cf. Fig. 12), one finds, quite surprisingly, that the typical lens mass is now boosted to around $0.8M_{\odot}$, a factor of 3–5 times larger than the value in more realistic models. Fig. 12 also shows that the theoretical predictions can not distinguish very well between a model with $0.075M_{\odot}$ lenses and a model with the lenses being twice as massive when different bulge/bar axis ratio, orientation and rotation speed are considered. We conclude that the fraction of

brown dwarfs in the Bulge is also sensitive to uncertainties from the dynamical model.

There are two sources of non-uniqueness of the dynamical model. The first is the shear transformation. Its effect on the distribution $f(\log t)$ of event durations is generally weak, typically at the 10% level in terms of the total rate (cf. Fig. 7). Also, as detailed analysis of the COBE map indicates, the shear transformation generally leaves detectable signatures in the left-to-right asymmetry map of the COBE map due to perspective effects (Binney et al. 1997, Zhao 1997 and references therein). The second source of non-uniqueness is the variety of velocity structures that are possible in the same bar. This non-uniqueness cannot be constrained from the COBE map. As shown also in Fig. 7, it can create typically about 20% difference in the event rate when one compares a stationary bar with a Jacobi-type rotating bar. This kind of non-uniqueness is potentially dangerous.

Most relevant to the lens mass function in the bar is the event duration distribution at the short event side. In particular, the mass moment $\frac{1}{m^2}$ (cf. eq. 51) is very sensitive to the velocity structure and the shear, and can easily vary by a factor of 2–3. This translates to an uncertainty of the lens mass (particularly at the lower end) by a factor about 1.4–1.7. This implies that any prediction on the faint end of the lens mass function in the bar is sensitive to details of the adopted dynamical model of the Galactic bar.

It is possible to reduce the non-uniqueness by fitting the stellar radial/proper motion velocity of the bar stars. In fact for the Freeman bar, it is possible to lift all the degeneracy if one can measure the line of sight mean streaming motion and velocity dispersion. For more realistic three-dimensional models, the non-uniqueness of the phase space structure is more complicated, and must be constrained by detailed numerical modeling. Generally one would need to fit radial velocities and proper motions at a number of positions of the bar. Combined with the COBE map and the microlensing optical depth, these data will strongly (if not uniquely) limit the axis ratio, the angle of the bar and the pattern speed.

It is a pleasure to thank Ken Freeman and Simon White for useful comments, and Dave Syer for help in programming with Mathematica. The careful scrutiny by the referee allowed us to improve the presentation. HSZ gratefully records the hospitality of the Max-Planck Institute in Garching where part of this work was done.

APPENDIX A: ORBIT BOUNDARIES

In the frame corotating with the bar the curves bounding the area filled by an orbit of the Freeman bar can be written in parameterized form using eqs (31–33) of F66. We find

$$X(\theta) = \frac{1}{A^2} + \frac{k^2 \theta^2}{k^4 A^2} \quad \# \quad (A1)$$

$$Y(\theta) = \frac{1}{k^4 A^2} + \frac{\theta^2}{k^2 A^2} \quad ; \quad \# \quad (A2)$$

where the $\#$ sign indicates the outer and inner boundaries,

$$\theta = A \cos \phi; \quad \phi = k A \sin \phi; \quad (A3)$$

and the parameter ϕ is an angle ranging between 0 and 2π . All quantities have the same meaning as in F66.

APPENDIX B: DERIVATION OF THE EVENT DURATION DISTRIBUTION

The distribution of the relative lens-source speed is integrated to be (cf. eq. [19])

$$F(V) = \max[0; Q(V)] + \max[0; Q(-V)]; \quad (B1)$$

where

$$4w_s w_l Q(V) = \min[w_s; w_l + v_{ls} - V] + \min[w_s; w_l - v_{ls} + V]; \quad (B2)$$

and $v_{ls} = v_l - v_s$. Apply the following change of variables to eq. (26)

$$\mathbf{x}_s = d(y) \sin \theta_s; \quad \mathbf{x}_l = d(y) \sin \theta_l; \quad (B3)$$

define θ and ϕ as in eq. (29), and write

$$\sin \theta_s = \sin \theta_l; \quad \theta = \phi; \quad (B4)$$

then

$$w_{s;l} = \frac{p-3}{3} (y) \cos \theta_{s;l}; \quad v_{s;l} = (y) \sin \theta_{s;l}; \quad (B5)$$

and

$$\theta_{s;l} = \frac{3M}{2ab} \left(1 - \frac{y^2}{y_0^2}\right) \cos \theta_{s;l}; \quad \frac{V}{(y)} = 2^{-1} p - ; \quad (B6)$$

It follows that (cf. eq. 26)

$$\frac{1}{f}(\log t) = \frac{2 \ln 10}{(t)^2} \frac{I_1(\theta; t)}{I_2}; \quad (B7)$$

where

$$I_1(\theta; t) = \int_{\theta=0}^{\theta=2\pi} \int_{\theta_s=0}^{\theta_s=2\pi} d\theta_s d\theta_l \cos^2 \theta_s \cos^2 \theta_l \quad (B8)$$

$$(\max[0; F_0(\theta; \theta_s; \theta_l)] + \max[0; F_0(\theta; \theta_s; \theta_l)]);$$

and

$$I_2 = \int_{\theta=0}^{\theta=2\pi} \int_{\theta_s=0}^{\theta_s=2\pi} d\theta_s d\theta_l \cos^2 \theta_s \cos^2 \theta_l = \frac{32}{45}; \quad (B9)$$

Here we have defined

$$F_0(\theta; \theta_s; \theta_l) = \frac{(t)VQ(V)}{p-p-3} \quad (B10)$$

$$= \frac{6 \cos \theta_s \cos \theta_l}{\min[\cos \theta_s; \cos \theta_l - H_0] + \min[\cos \theta_s; \cos \theta_l + H_0]};$$

where

$$H_0 = \frac{1}{p-3} \left(1 + \frac{p-3}{2}\right); \quad (B11)$$

Clearly I_1 is generally a dimensionless function of θ and t only, so that

$$\frac{1}{f}(\log t) = g(\theta) = \frac{45 \ln 10}{16 (t)^2} I_1(\theta; t); \quad (B12)$$

The asymptotic relations (cf. eqs 32 and 33) can be derived by letting $\theta \rightarrow 0$ and $\theta \rightarrow \pi$ for $t \rightarrow 0$, and $\theta \rightarrow \pi/2$ for $t \rightarrow 1$.

REFERENCES

- Alard C. et al., 1995, *The Messenger*, 80, 31
- Acock C., et al. 1997, *ApJ*, 479, 119
- Binney J.J., Gerhard O.E., Spiegel D.N., 1997, *MNRAS*, 288, 365
- Binney J.J., Tremaine S.D., 1987 *Galactic Dynamics* (Princeton Univ. Press).
- de Zeeuw P.T., 1993, *IAU Symposium 153, Galactic Bulges*, eds H. Dejonghe & H.J. Habing (Dordrecht: Kluwer), p. 191
- Dwek E., et al., 1995, *ApJ*, 445, 716
- Freeman K.C., 1966, *MNRAS*, 134, 15 (F66)
- Gerhard O.E., 1996, *IAU Symposium 165, Unsolved Problems in the Milky Way*, eds L. Blitz & P. Teuben (Dordrecht: Kluwer), p. 79
- Gould A., Bahcall J., Flynn C., 1996, *ApJ*, 465, 759
- Han C., Gould A., 1996, *ApJ*, 467, 540
- Han C., Lee S., 1997, *ApJ submitted* (astro-ph/9705137)
- Hunter C., 1974, *MNRAS*, 166, 633
- Kalnajs A.J., 1976, *ApJ* 205, 745 & 751
- Kiraga M., Paczynski B., 1994, *ApJ*, 430, L101
- Mao S., Paczynski B., 1996, *ApJ*, 473, 57
- Paczynski B., 1991, *ApJ*, 371, L63
- Paczynski B., 1996, *ARA A*, 34, 419
- Pfenniger D., 1984, *A & A*, 141, 171
- Tremaine S.D., 1976, *MNRAS*, 175, 557
- Udalski A., et al., 1994, *AcA*, 44, 165
- Weinberg M. & Tremaine S.D., 1983, *ApJ*, 271, 586
- Zhao H.S., 1996, *MNRAS*, 283, 149
- Zhao H.S., 1997, *MNRAS*, submitted
- Zhao H.S., Rich R.M., Spiegel D.N., 1996, *MNRAS*, 282, 175
- Zhao H.S., Spiegel D.N., Rich R.M., 1995, *ApJ*, 440, L13 (ZSR 95)
- Zhao H.S., Mao S., 1996, *MNRAS*, 283, 1197 (ZM)

This paper has been produced using the Royal Astronomical Society/Blackwell Science \LaTeX style file.